Time evolution of contact-angle dynamics for water and sodium chloride solution droplets during evaporation

Madaminov Ikromjon Baxtiyor o'g'li

Department of Physics, Faculty of Physics and Mathematics, Fergana State University, Fergana 150100, Uzbekistan.

Received 9 March 2026; accepted 28 April 2026

In this work, the time evolution of the contact-angle dynamics of distilled water droplets and 0.9% sodium chloride solution droplets placed on a solid glass surface was investigated experimentally during evaporation. The contact angle was determined using a simple geometric approach based on spherical-cap geometry from the droplet height and base diameter, without employing complex optical goniometric systems. The experiments were conducted under controlled environmental conditions, and the time-dependent variation of the contact angle was analyzed in detail. The results show that, for the 0.9% sodium chloride solution droplet, the contact angle decreases faster and in an almost monotonic manner compared with the distilled water droplet. In contrast, the water droplet exhibits stick–slip behavior associated with contact-line pinning and depinning processes. The obtained results indicate that electrolyte ions influence wetting properties and contact-line dynamics. This study demonstrates the applicability of a simple geometric approach for contact-angle analysis without using complex goniometric systems. Furthermore, the obtained results for the 0.9% NaCl solution may serve as useful reference data for modeling the evaporation behavior of physiological saline droplets on solid substrates.

Keywords: Contact angle; droplet evaporation; water; sodium chloride solution; wetting dynamics.

DOI: https://doi.org/10.31349/RevMexFis.72.050601

1. Introduction

Evaporation of liquid droplets placed on a solid surface is one of the fundamental processes closely related to the physics of surface phenomena, heat and mass transfer, and wetting dynamics [1–3]. Such processes play an important role in many practical applications, including coating technologies, inkjet printing systems, microfluidics, biological assays, and materials processing [2, 4]. A macroscopic description of sessile-droplet evaporation is commonly based on the droplet geometry and its time evolution, where the contact angle emerges as a key physical parameter [3].

The contact angle is defined at the three-phase contact line where the liquid, solid surface, and gas phase meet, and it characterizes the degree of wetting of a surface by a liquid. Under equilibrium conditions, it is determined by the balance of interfacial tensions and is expressed by the classical Young equation [1]. However, during evaporation the droplet deviates from equilibrium; as a consequence, both the contact angle and the position of the contact line change dynamically with time [3–5]. Therefore, investigating the time-dependent evolution of the contact angle is necessary for a complete characterization of sessile-droplet evaporation [4, 5].

In previous studies, droplet evaporation is often interpreted in terms of two ideal limiting regimes: a constant contact radius (CCR) mode, in which the contact radius remains nearly unchanged while the contact angle decreases, and a constant contact angle (CCA) mode, in which the contact angle remains approximately constant while the contact line recedes [2, 3]. Under practical conditions, evaporation frequently proceeds in an intermediate, i.e., hybrid regime between these two limits. In this case, temporary arrest and subsequent motion of the contact line are described by pinning–depinning processes, which lead to a nonlinear evolution of the contact angle [4, 6].

Many investigations of sessile-droplet evaporation have primarily focused on pure water droplets. These studies show that the evaporation rate and contact-angle dynamics of water droplets depend significantly on substrate properties, temperature, and relative humidity [3, 5]. In addition, a nonuniform distribution of evaporative flux along the droplet surface can induce internal capillary flows, thereby modifying the droplet shape and evaporation kinetics. This phenomenon has been widely studied in connection with the "coffee-ring" effect [5].

Compared to pure water, evaporation of electrolyte-solution droplets has been investigated to a lesser extent. The presence of ions in solution alters surface tension, vapor pressure, and wetting conditions, and can lead to the formation of concentration gradients inside the droplet during evaporation [7, 8]. As evaporation proceeds, the increasing salt concentration causes a redistribution of interfacial forces, which differentiates the contact-line dynamics and contact-angle evolution from the pure-water case both qualitatively and quantitatively [7, 9].

In this context, an aqueous sodium chloride solution with a concentration of 0.9% is of particular interest. This specific concentration corresponds to standard physiological saline, making it highly relevant for medical and biological applications. Investigating the contact-angle dynamics of 0.9% NaCl droplets provides useful reference data for modeling the evaporation behavior of physiological saline droplets on solid surfaces.

In this work, the time evolution of the contact-angle dynamics of distilled water droplets and 0.9% NaCl solution droplets placed on a solid glass surface is experimentally studied and comparatively analyzed during evaporation. The contact angle is determined using a simple geometric method based on measurements of the droplet height and base diameter, which enables real-time monitoring without employing complex optical goniometric systems. The main objective of this study is to identify differences in the contact-angle evolution between water and electrolyte-solution droplets and to experimentally evaluate the influence of ions on wetting and evaporation mechanisms.

2. Experimental setup and methods

2.1. Experimental setup and conditions

This study was carried out using a laboratory setup designed to investigate the contact-angle dynamics of sessile droplets during evaporation on a solid surface. Distilled water droplets and 0.9% sodium chloride (NaCl) solution droplets, known as physiological saline, were selected as experimental objects due to their biological relevance. The experiments were performed on a smooth and transparent glass substrate.

The droplets were deposited using an automatic piston micropipette with an initial volume of 5.5 μL, ensuring a stable shape close to a spherical cap (Fig. 1). To ensure minimal kinetic energy, the liquid was slowly extruded until a hanging drop gently made contact with the surface, effectively preventing splashing or artificial spreading.

The experiments were conducted in a specially constructed isolation chamber protected from external airflow and vibrations. To ensure thermal stability, the inner walls were lined with heat-reflecting foil. All experimental runs were performed at a constant ambient temperature of 23 ± 0.5 °C, maintained by a controlled heating panel and monitored using a digital thermohygrometer to ensure stable evaporation kinetics. Under these sealed and thermally regulated conditions, the relative humidity naturally stabilized at approximately 30%. Maintaining a strictly constant relative humidity is critical, as evaporation kinetics and contact-angle dynamics are highly sensitive to ambient moisture levels. By conducting all measurements at this stable 30% humidity baseline, the comparison between the two liquids was performed under identical environmental conditions. The general view of the experimental setup is shown in Fig. 2.

FIGURE 1. Automatic piston micropipette used for forming droplets and dispensing them onto the substrate surface (initial volume: 5.5 μL).

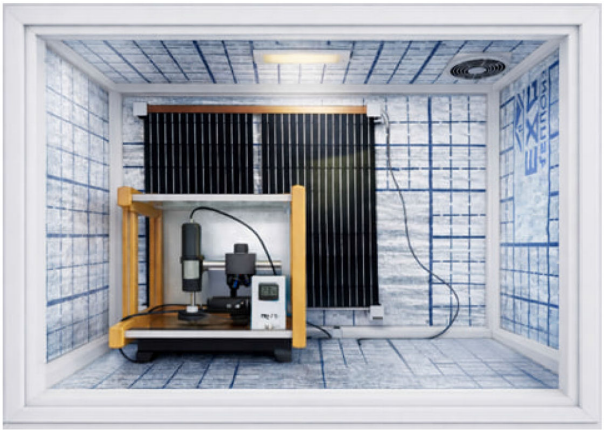

FIGURE 2. General view of the experimental setup designed to observe sessile-droplet evaporation under controlled conditions (isolated environment and arrangement of the measurement system).

FIGURE 3. Digital USB microscope system used for acquiring droplet images during evaporation. This figure illustrates the imaging device only; quantitative geometric measurements were performed on calibrated digital images, as shown in Fig. 4.

2.2. Observation and measurement of droplet geometry

The droplet evaporation process was observed from the side using a digital microscope (Fig. 3). The microscope enabled real-time imaging of the droplet side profile, while the droplet geometric parameters were determined from calibrated digital images (Fig. 4). During the experiments, the digital microscope was set to a fixed magnification of approximately 100x. This specific magnification level was chosen to ensure a clear, high-resolution view of the three-phase contact line while keeping the entire droplet profile within the field of view. Images of the evaporating droplet were acquired continuously at a fixed recording interval of 1 frame per minute (*i.e.*, one image every 60 seconds).

This specific acquisition interval was chosen to provide sufficient temporal resolution to accurately track the relatively slow macroscopic changes in the droplet profile and contact angle throughout the entire evaporation process.

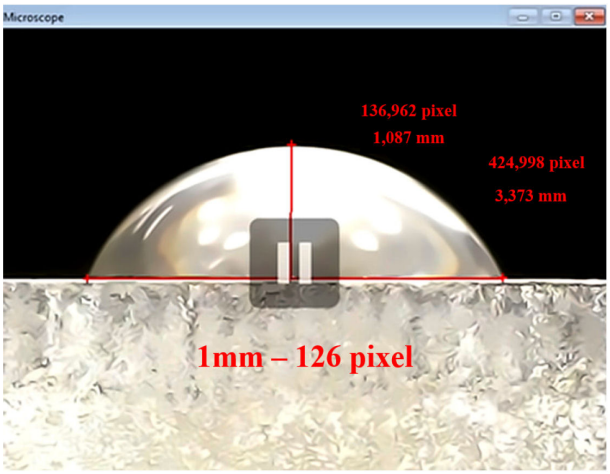

FIGURE 4. Example of measuring the droplet base diameter d and height h in the calibrated microscope image. The calibration factor was 1 mm = 126 pixels.

The droplet geometric parameters—the base radius r at the droplet–substrate contact and the height h from the substrate surface to the droplet apex—were determined at each time interval during the evaporation process. To extract the geometric parameters, the acquired images were processed using the microscope's dedicated measurement software, which was carefully calibrated using a standard micrometer scale prior to the experiments. Under the selected imaging conditions, the calibration factor was determined as 1 mm = 126 pixels, which was used to convert pixel-based measurements into physical units. The image processing steps involved first defining the solid-liquid baseline (the substrate surface). Then, the base diameter d was determined by manually identifying and marking the two distinct three-phase contact points on this baseline. Following this, the droplet height h was measured by drawing a perpendicular vertical line from the center of the baseline to the highest boundary point (apex) of the droplet profile. These specific measurement steps were systematically repeated for each acquired frame to extract the continuous parameters required for the contact angle calculation.

The microscope system was calibrated in advance to ensure that all measurements were performed at the same scale. The proximity of the droplet shape to a spherical cap was visually monitored, and cases with noticeable geometric deviations were excluded from the analysis.

2.3. Method for determining the contact angle

To determine the contact angle, the droplet shape was treated as a spherical cap. This approach is justified by the fact that, for the selected droplet volume, surface-tension forces strongly dominate over gravitational effects. Quantitatively, this assumption is validated by evaluating the Bond number (Bo), which represents the ratio of gravitational forces to surface tension forces: $Bo = \rho g R^2/\gamma$, where ρ is the liquid density, g is the gravitational acceleration, R is the droplet base radius, and γ is the surface tension. The physical properties of the liquids used in the experiments were determined at the controlled temperature of 23°C. For distilled water, the density was $\rho = 997.5$ kg/m^3 and the surface tension was $\gamma = 72.3$ mN/m. For the 0.9% NaCl solution, the density and surface tension were slightly higher, at $\rho = 1004.6$ kg/m^3 and $\gamma = 72.8$ mN/m, respectively. These values were utilized to evaluate the Bond number (Bo), which characterizes the ratio of gravitational to surface-tension forces. For the distilled water droplet, taking $\rho = 1000$ kg/m^3, $\gamma \approx 72$ mN/m, and the maximum measured initial base radius $R \approx 1.69$ mm, the calculated Bond number is $Bo \approx 0.39$. Additionally, the capillary length $l_c = \sqrt{\gamma/\rho g}$ for water is approximately 2.71 mm. Since the initial droplet radius (1.69 mm) is strictly less than the capillary length, and the Bond number is well below unity ($Bo < 1$), gravitational flattening is negligible. Thus, the droplet firmly resides in the capillary regime, ensuring that its shape accurately conforms to a spherical cap throughout the evaporation process. Deviations from the spherical shape would only occur for significantly larger droplets where $Bo > 1$. The droplet side profile was analyzed in the plane as a part of a circular arc. Based on the droplet geometry, the contact angle θ is determined from the droplet height h and the base diameter d using the following expression:

$$\theta = \arccos\left(\frac{d^2 - 4h^2}{d^2 + 4h^2}\right). \tag{1}$$

This formula makes it possible to determine the angle between the tangent line to the droplet surface at the point of contact with the substrate and the substrate plane. The applied geometric method, based on the spherical-cap approximation, is a well-established technique in the study of wetting phenomena, particularly when surface tension dominates over gravity [2, 3]. Compared to more complex approaches such as polynomial fitting of the droplet profile or professional optical goniometry, this height-width method offers a practical and robust alternative for real-time monitoring under controlled laboratory conditions. It eliminates the need for sophisticated image-analysis algorithms while maintaining high accuracy for small sessile droplets ($Bo < 1$), where the profile remains inherently circular. Similar geometric approaches have been successfully utilized in previous studies to evaluate the evaporation kinetics of pure and multicomponent liquid droplets on various substrates [3, 4]. During the evaporation process, the contact angle was recalculated at each time point, and its time evolution was analyzed.

2.4. Data processing

To ensure a precise evaluation of the temporal resolution, the geometric parameters were extracted and the contact angle was calculated at a strict time interval of 1 minute between consecutive analyzed images. This consistent 1-minute temporal resolution was maintained throughout the entire duration of the evaporation process for both liquids. The ex-

periments were carried out under controlled laboratory conditions, with the relative humidity maintained at approximately 30%. The obtained results were used to identify general trends in contact-line behavior, including monotonic and nonuniform decreasing regimes, as well as possible pinning and depinning effects. The presented data correspond to representative measurements obtained under the same experimental conditions for both liquids. To ensure the reproducibility of the experimental results, each evaporation test for both distilled water and 0.9% NaCl solution was repeated three times under identical environmental conditions ($23 \pm 0.5°$C and 30% RH). The data points presented in the results section correspond to the representative average values obtained from these runs. The maximum relative uncertainty in the determination of the contact angle was estimated to be approximately $\pm 1.5°$, which primarily originates from the manual identification of the three-phase contact points and the substrate baseline during the digital image processing stage.

3. Results and discussion

3.1. Time evolution of the contact angle for a distilled water droplet

The visual evolution of the distilled water droplet profile during the 45-minute evaporation period is presented in Fig. 5. As observed, the droplet maintains a shape close to a spherical cap while both its height h and base diameter d decrease progressively over time. These side-profile images provide direct visual evidence of the geometric changes discussed in the following analysis.

During the evaporation of a distilled water droplet, the time variation of the contact angle θ was monitored over the interval $0 - 45$ min. At the initial state, the droplet had a geometry close to a spherical cap, and at $t = 0$ min the contact angle was $\theta \approx 65.19°$. As evaporation proceeded, the droplet height h and the base radius r (diameter d) decreased steadily, and consequently $\theta(t)$ showed an overall decreasing trend.

At each time point, the contact angle was calculated from the droplet geometric parameters using the geometric method described above according to Eq. (1).

The measured base diameter, height, and the calculated contact-angle values for the water droplet are presented in Table I.

The time evolution of the contact angle for the distilled water droplet is presented in Fig. 6 (orange curve). The general trend of the curve indicates that the contact angle decreases with time; however, this decrease is not strictly linear over the entire process. In several time intervals, the rate of decrease becomes slower, and small short-term deviations from the overall trend are observed. Such behavior is consistent with possible contact-line pinning and depinning ("stick–slip") effects, which are commonly encountered during sessile-droplet evaporation on solid substrates. These local deviations become more evident during the transition from a stage in which the contact line remains nearly pinned, corresponding approximately to the CCR regime, to a stage in which contact-line motion becomes more noticeable.

From a practical point of view, the evaporation process of the water droplet may be qualitatively divided into three stages. In the initial stage, the contact angle decreases relatively rapidly while the contact radius remains nearly stable, which is characteristic of behavior close to the CCR regime. In the intermediate stage, the decrease of θ becomes slower and stick–slip-like features appear more clearly, indicating alternating periods of temporary pinning and partial motion of the contact line. In the final stage, the droplet becomes flatter and the contact angle decreases more sharply as the droplet volume approaches its final stage of evaporation. These stages may be associated with the coupling between droplet geometry, evaporative mass loss, and contact-line dy-

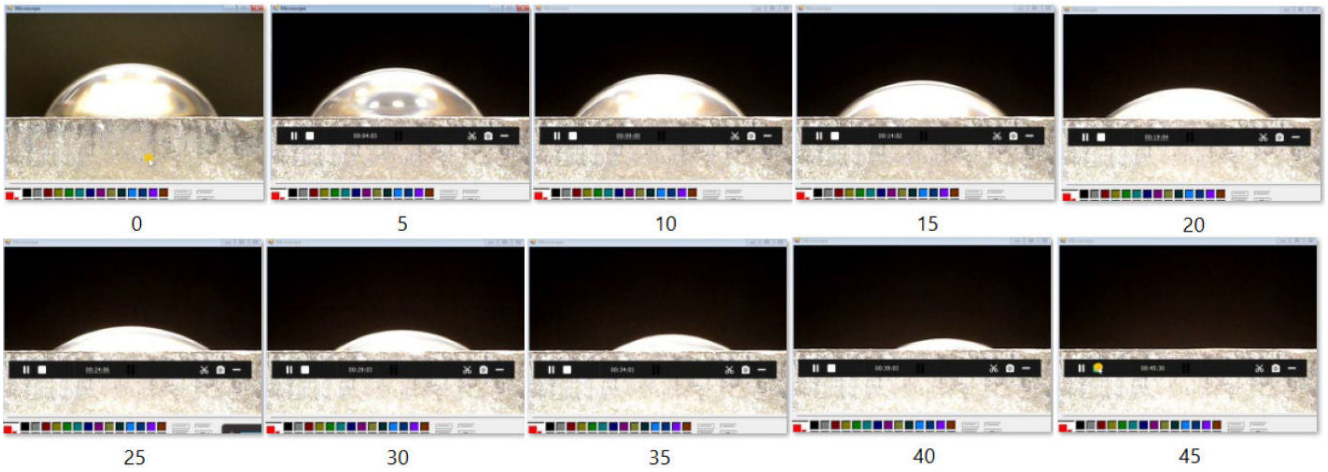

FIGURE 5. Side-profile microscope images of a distilled water droplet at representative time intervals (from $t = 0$ to $t = 45$ min) during evaporation on a glass surface at 23°C.

TABLE I. Time-dependent values of the geometric parameters and the contact angle θ during evaporation of a distilled water droplet.

Time (min)	Diameter (mm)	Height (mm)	θ (°)	Time (min)	Diameter (mm)	Height (mm)	θ (°)
0	3.381	1.081	65.194	23	3.095	0.508	36.347
1	3.373	1.040	63.321	24	3.048	0.484	35.238
2	3.365	1.016	62.252	25	3.016	0.460	33.928
3	3.357	0.992	61.167	26	2.976	0.445	33.300
4	3.349	0.960	59.652	27	2.929	0.437	33.230
5	3.333	0.929	58.275	28	2.794	0.429	34.142
6	3.325	0.905	57.124	29	2.651	0.413	34.612
7	3.317	0.889	56.385	30	2.571	0.397	34.324
8	3.310	0.865	55.188	31	2.524	0.365	32.262
9	3.302	0.849	54.428	32	2.437	0.349	31.965
10	3.302	0.833	53.546	33	2.389	0.341	31.865
11	3.294	0.786	51.024	34	2.333	0.325	31.137
12	3.286	0.778	50.677	35	2.262	0.317	31.315
13	3.286	0.730	47.912	36	2.119	0.278	29.405
14	3.270	0.714	47.182	37	2.064	0.262	28.490
15	3.262	0.691	45.921	38	1.944	0.222	25.731
16	3.254	0.651	43.615	39	1.873	0.206	24.811
17	3.254	0.635	42.640	40	1.786	0.199	25.126
18	3.246	0.619	41.753	41	1.746	0.159	20.644
19	3.238	0.587	39.858	42	1.675	0.127	17.245
20	3.214	0.571	39.122	43	1.587	0.103	14.792
21	3.190	0.548	37.923	44	1.524	0.087	13.027
22	3.119	0.532	37.673	45	1.111	0.040	8.237

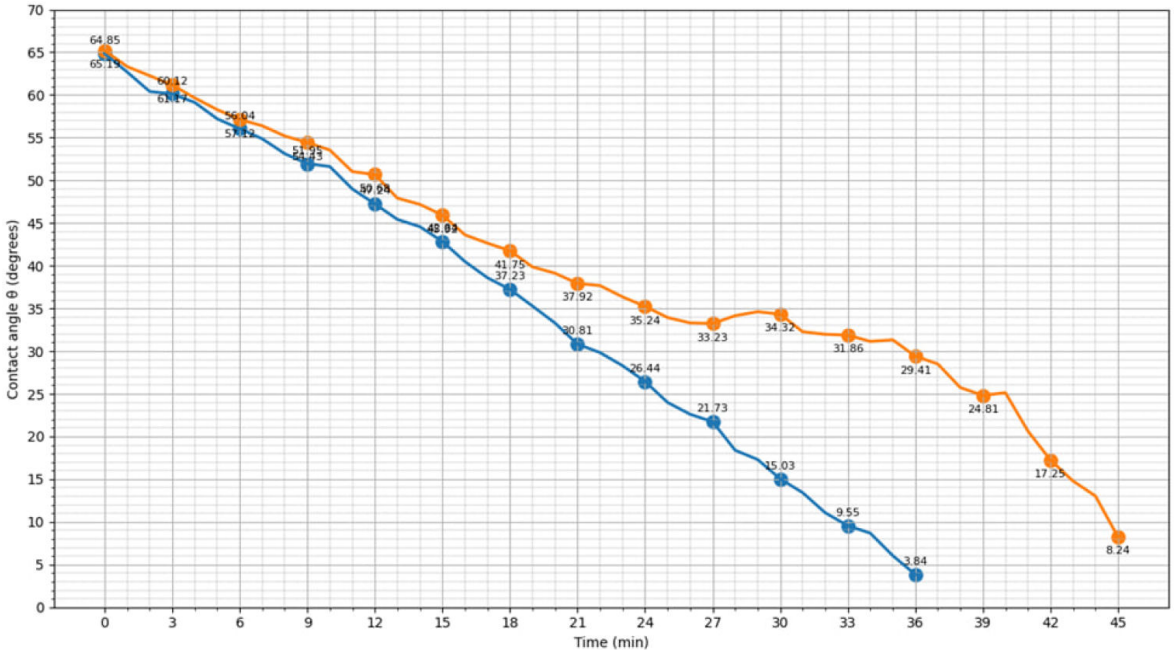

FIGURE 6. Comparative time evolution of the contact angle θ for distilled water (orange symbols) and 0.9% NaCl solution (blue symbols) droplets during evaporation.

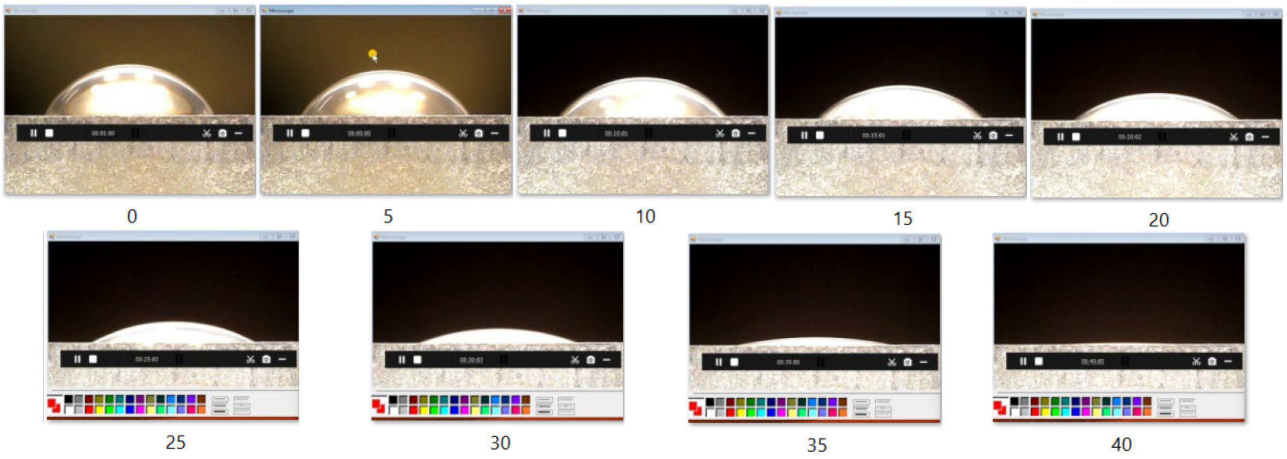

FIGURE 7. Side-profile microscope images of a 0.9% NaCl solution droplet at representative time intervals (from $t = 0$ to $t = 40$ min) during evaporation, showing the characteristic pinning behavior.

namics. Thus, the water droplet exhibits a nonuniform evolution of the contact angle that reflects the complexity of the evaporation process even under controlled laboratory conditions. The observation of the distilled water droplet was concluded at 45 minutes. At this stage, the droplet had entered its final phase of evaporation, characterized by an extremely low height ($h \approx 0.040$ mm) and a very small contact angle ($\theta \approx 8.24°$). Beyond this point, the droplet effectively becomes a thin, non-uniform liquid film where the spherical-cap geometry is no longer a valid approximation for precise contact-angle calculation. This endpoint is justified by the physical limits of the measurement technique, as the droplet profile transitions from a well-defined cap to a residual liquid layer.

3.2. Contact-angle dynamics for the 0.9% NaCl solution droplet

Figure 7 illustrates the side-profile evolution of the 0.9% NaCl solution droplet during a 40-minute observation period. In contrast to pure water, the saline droplet exhibits a more pronounced pinning of the contact line, where the base diameter remains nearly constant for a longer duration while the height and contact angle decrease more sharply. This behavior is visually evident in the later stages of the evaporation process.

For the 0.9% NaCl solution droplet, the contact-angle evolution was measured over the interval 0–36 min. At the initial time, $\theta \approx 64.85°$, indicating that the initial contact angle is very close to that of the distilled water droplet under the same experimental conditions. This similarity at the beginning of the experiment makes it possible to compare the subsequent evaporation behavior of the two droplets on a common basis. However, during the later stages of the process, the contact angle of the NaCl solution droplet decreases more rapidly than that of the water droplet and, by the end of the experiment, reaches the regime of very small angles. This behavior suggests that the temporal evolution of the droplet geometry is more pronounced in the presence of the saline solution. The measured geometric parameters and the corresponding calculated contact-angle values for the NaCl solution droplet are presented in Table II.

The contact angle dynamics for the NaCl solution are compared with water in Fig. 6 (blue curve). For the NaCl droplet, the decrease of $\theta(t)$ is smoother and almost monotonic compared with the water droplet, and short-term deviations are less pronounced. This suggests that, in the presence of the NaCl solution, the contact-line dynamics may differ from those observed for the water droplet. As evaporation proceeds, the increase in concentration may modify interfacial interactions and wetting conditions, which could contribute to a faster reduction of the contact angle.

3.3. Comparative analysis of distilled water and 0.9% NaCl droplets

To directly compare the contact-angle dynamics of the water and NaCl droplets, Fig. 6 shows the combined $\theta(t)$ curves for both droplets in a single coordinate system. The presented curves correspond to representative measurements obtained under identical experimental conditions for both liquids. The comparative analysis shows that, although the initial contact angles are almost equal, at later stages of evaporation the contact angle of the NaCl solution droplet decreases faster than that of the water droplet and enters the small-angle regime much earlier. In the water droplet, the $\theta(t)$ curve exhibits more pronounced stick–slip-like features. This difference may be related to the influence of NaCl ions on surface tension, wetting behavior, and concentration changes occurring during evaporation.

3.4. Discussion of physical mechanisms

The obtained results suggest that the time evolution of the contact angle during evaporation is closely related to contact-line dynamics, interfacial interactions, and the redistribution of mass within the droplet. For the distilled water droplet, the nonuniform character of the $\theta(t)$ curve and the presence of

TABLE II. Time-dependent values of the geometric parameters and the contact angle θ during evaporation of a 0.9% NaCl solution droplet.

Time (min)	Diameter (mm)	Height (mm)	θ (°)	Time (min)	Diameter (mm)	Height (mm)	θ (°)
0	3.397	1.079	64.85285	19	3.246	0.516	35.27402
1	3.389	1.032	62.68527	20	3.238	0.484	33.28807
2	3.381	0.984	60.40534	21	3.230	0.445	30.81021
3	3.373	0.976	60.11708	22	3.222	0.429	29.82299
4	3.357	0.952	59.12148	23	3.214	0.405	28.29050
5	3.349	0.913	57.20174	24	3.175	0.373	26.44483
6	3.341	0.889	56.04167	25	3.135	0.333	23.98724
7	3.333	0.865	54.86331	26	3.103	0.310	22.59856
8	3.333	0.833	53.11635	27	3.064	0.294	21.72666
9	3.325	0.810	51.95236	28	3.040	0.246	18.38632
10	3.317	0.802	51.61399	29	3.024	0.230	17.29864
11	3.310	0.754	48.98699	30	3.016	0.199	15.03496
12	3.302	0.722	47.24055	31	2.976	0.175	13.41521
13	3.302	0.691	45.42196	32	2.952	0.143	11.06749
14	3.294	0.675	44.57118	33	2.849	0.119	9.550584
15	3.278	0.643	42.84138	34	2.714	0.103	8.681166
16	3.270	0.603	40.48869	35	2.690	0.071	6.043462
17	3.262	0.571	38.58948	36	2.389	0.040	3.835873
18	3.254	0.548	37.22872				

short-term deviations are consistent with intermittent pinning and depinning of the contact line. Such behavior is typical of evaporation in a mixed or hybrid regime between the constant contact radius (CCR) and constant contact angle (CCA) limits, where temporary fixation of the contact line is followed by partial motion of the contact perimeter. In the initial stage of evaporation, the behavior of the water droplet is close to the CCR regime, since the contact angle decreases while the contact radius remains nearly unchanged. At later stages, the appearance of local deviations and more noticeable contact-line motion suggests a transition toward a hybrid evaporation regime.

For the 0.9% NaCl solution droplet, the decrease of the contact angle is smoother and closer to a monotonic trend. This behavior suggests that the presence of dissolved ions modifies the interfacial conditions and the mobility of the contact line. As evaporation proceeds, the local salt concentration near the contact line increases because the evaporative flux is generally higher near the droplet edge. This concentration increase may affect both the local surface tension and the balance of adhesive forces acting at the three-phase boundary. As a consequence, the contact-line dynamics may differ from those of the pure-water droplet, and the observed evolution becomes less irregular.

A possible physical interpretation is that the redistribution of ions during evaporation changes the coupling between surface tension, concentration gradients, and contact-line mobility. In evaporating saline droplets, concentration gradients may develop between the droplet center and the peripheral region, especially at later stages of evaporation. Such gradients can modify the local interfacial state and can contribute to a smoother recession of the droplet profile. In this sense, the faster decrease of the contact angle observed for the NaCl solution may be related not only to evaporation itself, but also to concentration-dependent changes in wetting behavior. This interpretation is consistent with previous studies showing that solute accumulation near the contact-line region can modify interfacial conditions and influence pinning–depinning behavior in evaporating saline droplets [8, 9].

In the saline droplet, evaporation leads to a gradual increase in salt concentration, particularly near the droplet edge where the evaporative flux is higher. This localized solute accumulation can enhance contact-line pinning and keep the droplet base nearly constant for a longer period, corresponding to behavior close to the CCR mode. Under such conditions, mass loss occurs while the contact line remains relatively constrained; therefore, the contact angle decreases more sharply in order to preserve the spherical-cap geometry. This interpretation also explains why the faster decrease of $\theta(t)$ in the 0.9% NaCl droplet should not be directly attributed to a higher volumetric evaporation rate. Although dissolved ions may slightly reduce the vapor pressure and thus tend to slow evaporation, the observed $\theta(t)$ evolution is mainly associated with stronger three-phase contact-line pinning. In contrast, the distilled water droplet exhibits more frequent depinning events, which allows the contact angle to decrease at a slower overall rate.

The present observations are qualitatively consistent with previous studies on sessile-droplet evaporation. In particular, the nonuniform evaporation of pure-water droplets and

the importance of pinning–depinning effects are in agreement with the general framework described for evaporating droplets on solid substrates [2–4]. In addition, the role of saline content in modifying evaporation behavior and interfacial processes is consistent with reports on evaporating salt-solution droplets [7–9]. At the same time, the present work differs from many previous studies in that the contact-angle evolution is determined here by a simple geometric method based on direct measurements of droplet height and base diameter, without the use of complex optical goniometric systems. While previous models often focus on pure liquids, the main contribution of this study is the systematic evaluation of electrolyte influence on contact-line pinning using an accessible yet robust geometric approach. By bridging the gap between complex theoretical models and practical laboratory measurements, this research establishes a reliable framework for studying the wetting dynamics of saline solutions at physiologically relevant concentrations, which has remained less explored in recent literature.

4. Conclusion

A quantitative comparison of the evaporation kinetics reveals that the 0.9% NaCl solution droplet reaches the low-contact-angle regime ($\theta < 10^\circ$) significantly faster than the distilled water droplet. Specifically, the saline droplet achieves this state at $t = 33$ min, while the water droplet requires approximately 44 min to reach a comparable angle, representing a 25% reduction in the total duration of the spherical-cap stage. This accelerated decrease in $\theta(t)$ is consistent with the findings of Shahidzadeh *et al.* [8], who observed that solute accumulation at the contact line restricts the recession of the droplet base, thereby forcing a steeper decline in the contact angle to accommodate volume loss. Furthermore, the stick–slip behavior observed in our pure water samples, characterized by contact angle fluctuations of up to 2°–3° (*e.g.*, between $t = 27$ and $t = 30$ min), is markedly absent in the saline droplets, where the ions effectively stabilize the three-phase boundary. These observations provide a more detailed quantitative description of how electrolyte concentration influences wetting dynamics compared with previous qualitative descriptions.

In this study, the time evolution of the contact angle θ for distilled water droplets and 0.9% NaCl solution droplets evaporating on a glass surface was investigated experimentally and comparatively analyzed. The contact angle was determined using a geometric approach based on the measured droplet parameters, and the $\theta(t)$ dynamics were evaluated at different stages of the evaporation process.

The experimental results showed that, for both liquids, the contact angle follows an overall decreasing trend during evaporation. However, the evolution of the contact angle appears to depend on the liquid composition. For the distilled water droplet, the variation of $\theta(t)$ is nonuniform and shows features consistent with stick–slip-type contact-line behavior. In contrast, for the 0.9% NaCl solution droplet, the decrease of the contact angle is smoother and almost monotonic, and short-term fluctuations are less pronounced. These differences may be related to the influence of electrolyte ions on wetting conditions and contact-line dynamics.

The applied geometric approach makes it possible to determine the contact angle in real time using simple microscopic measurements, without employing complex optical goniometric systems. The obtained results show that this methodology is practically useful for comparative evaluation of wetting dynamics during sessile droplet evaporation and for analyzing the influence of electrolyte solutions on the contact-angle evolution under controlled conditions. A more detailed statistical analysis based on repeated measurements and uncertainty estimation will be considered in future work.

1. T. Young, An essay on the cohesion of fluids, *Phil. Trans. R. Soc. Lond.* **95** (1805) 65, https://doi.org/10.1098/rstl.1805.0005.
2. R. G. Picknett and R. Bexon, The evaporation of sessile or pendant drops in still air, *J. Colloid Interface Sci.* **61** (1977) 336, https://doi.org/10.1016/0021-9797(77)90396-4.
3. H. Hu and R. G. Larson, Evaporation of a sessile droplet on a substrate, *J. Phys. Chem. B* **106** (2002) 1334, https://doi.org/10.1021/jp0118322.
4. Y. O. Popov, Evaporative deposition patterns: Spatial dimensions of the deposit, *Phys. Rev. E* **71** (2005) 036313, https://doi.org/10.1103/PhysRevE.71.036313.
5. R. D. Deegan, O. Bakajin, T. F. Dupont, G. Huber, S. R. Nagel and T. A. Witten, Capillary flow as the cause of ring stains from dried liquid drops, *Nature* **389** (1997) 827, https://doi.org/10.1038/39827.
6. G. J. Dunn, S. K. Wilson, B. R. Duffy, S. David and K. Sefiane, The strong influence of substrate conductivity on droplet evaporation, *J. Fluid Mech.* **623** (2009) 329, https://doi.org/10.1017/S0022112008005004.
7. N. Shahidzadeh-Bonn, S. Rafai, D. Bonn and G. Wegdam, Salt crystallization during evaporation: Impact of interfacial properties, *Langmuir* **24** (2008) 8599, https://doi.org/10.1021/la8005629.
8. N. Shahidzadeh, M. F. L. Schut, J. Desarnaud, M. Prat and D. Bonn, Salt stains from evaporating droplets, *Sci. Rep.* **5** (2015) 10335, https://doi.org/10.1038/srep10335.
9. V. Soulié *et al.*, The evaporation behavior of sessile droplets from aqueous saline solutions, *Phys. Chem. Chem. Phys.* **17** (2015) 22296, https://doi.org/10.1039/C5CP02444G.